JCI The Journal of Clinical Investigation

# Abolition of aberrant neurogenesis ameliorates cognitive impairment after stroke in mice

María Isabel Cuartero, … , Ignacio Lizasoain, María Àngeles Moro

*J Clin Invest.* 2019. https://doi.org/10.1172/JCI120412.

**Research** In-Press Preview **Neuroscience**

Post-stroke cognitive impairment is considered one of the main complications during the chronic phase of ischemic stroke. In the adult brain, the hippocampus regulates both encoding and retrieval of new information through adult neurogenesis. Nevertheless, the lack of predictive models and studies based on the forgetting processes hinder the understanding of memory alterations after stroke. Our aim was to explore whether post-stroke neurogenesis participates in the development of long-term memory impairment. Here we show a hippocampal neurogenesis burst that persisted one month after stroke and that correlated with an impaired contextual and spatial memory performance. Furthermore, we demonstrate that the enhancement of hippocampal neurogenesis after stroke by physical activity or memantine treatment weakened existing memories. More importantly, stroke-induced newborn neurons promoted an aberrant hippocampal circuitry remodelling with differential features at ipsi- and contralesional levels. Strikingly, inhibition of stroke-induced hippocampal neurogenesis by temozolomide treatment or using a genetic approach (Nestin-Cre$^{ERT2}$/NSE-DTA mice) impeded the forgetting of old memories. These results suggest that hippocampal neurogenesis modulation could be considered as a potential approach for post-stroke cognitive impairment.



# ABOLITION OF ABERRANT NEUROGENESIS AMELIORATES COGNITIVE IMPAIRMENT AFTER STROKE IN MICE

María Isabel Cuartero,[1,2] Juan de la Parra,[1,2] Alberto Pérez-Ruiz,[1,2] Isabel Bravo-Ferrer,[1,2] Violeta Durán-Laforet,[1,2] Alicia García-Culebras,[1,2] Juan Manuel García-Segura,[2,3] Jagroop Dhaliwal,[4] Paul W. Frankland,[4] Ignacio Lizasoain,[1,2] María Ángeles Moro[1,2]

[1]Departamento de Farmacología y Toxicología, Facultad de Medicina, Universidad Complutense de Madrid (UCM), and Instituto de Investigación Hospital 12 de Octubre (i+12), Madrid, Spain.

[2]Instituto Universitario de Investigación en Neuroquímica (IUIN), UCM, Madrid, Spain.

[3]Departamento de Bioquímica y Biología Molecular, Facultad de Ciencias Químicas, UCM, Madrid, Spain.

[4]Program in Neuroscience & Mental Health, Hospital for Sick Children, 555 University Avenue, Toronto, ON M5G 1X8, Canada.

MIC's present address: Centro de Biología Molecular Severo Ochoa, CSIC, Spain.

MIC, JP and AP have equally contributed to this work.

**Address correspondence** to María A. Moro (neurona@med.ucm.es) or María Isabel Cuartero (maribel_cd@hotmail.com), Unidad de Investigación Neurovascular, Departamento de Farmacología y Toxicología, Facultad de Medicina, Universidad Complutense, Pza. Ramón y Cajal s/n, 28040 Madrid, Spain. Tel.: +34-913941452.

**Conflict of interest statement**: The authors have declared that no conflict of interest exists.

**ABSTRACT**

Post-stroke cognitive impairment is considered one of the main complications during the chronic phase of ischemic stroke. In the adult brain, the hippocampus regulates both encoding and retrieval of new information through adult neurogenesis. Nevertheless, the lack of predictive models and studies based on the forgetting processes hinder the understanding of memory alterations after stroke. Our aim was to explore whether post-stroke neurogenesis participates in the development of long-term memory impairment. Here we show a hippocampal neurogenesis burst that persisted one month after stroke and that correlated with an impaired contextual and spatial memory performance. Furthermore, we demonstrate that the enhancement of hippocampal neurogenesis after stroke by physical activity or memantine treatment weakened existing memories. More importantly, stroke-induced newborn neurons promoted an aberrant hippocampal circuitry remodelling with differential features at ipsi- and contralesional levels. Strikingly, inhibition of stroke-induced hippocampal neurogenesis by temozolomide treatment or using a genetic approach (Nestin-Cre$^{ERT2}$/NSE-DTA mice) impeded the forgetting of old memories. These results suggest that hippocampal neurogenesis modulation could be considered as a potential approach for post-stroke cognitive impairment.

## INTRODUCTION

Stroke is one of the leading causes of death and disability worldwide, affecting millions of lives every year. In the past few decades, advances in prevention and healthcare have progressively reduced stroke mortality (1). As a result, stroke can be now considered a chronically disabling disease with many stroke survivors displaying a range of motor, cognitive, and psychiatric impairments. Importantly, whereas motor impairment may ameliorate during the chronic phase of stroke, cognitive deficits tend to worsen (2, 3). In fact, more than 1/3 of patients may develop cognitive impairment or even dementia later after stroke (4-6). Despite this high prevalence, mechanisms underlying post-stroke cognitive impairment and dementia remain unclear (2, 4, 7).

The hippocampus is one of the main adult brain regions implicated in cognitive functions. Through adult neurogenesis, newborn neurons are continually added to the hippocampal circuits contributing to the encoding of new hippocampus-dependent memories (8). Nevertheless, since neuronal integration produces remodelling of pre-existing hippocampal circuitry, increasing neurogenesis also may promote the destabilization and even the clearance of previous stored memories (9). Indeed, alterations in neurogenesis and neuronal integration have been proposed to contribute to cognitive impairment (10-12) in different pathological scenarios such as epilepsy, schizophrenia and neurodegenerative diseases (for rev., see 8, 13).

Of note, stroke is known to trigger a strong neurogenic burst in the hippocampus (for rev., see 14, 15). Although subgranular zone (SGZ) neurogenesis could promote cognitive function recovery after cerebral ischemia (16, 17), stroke also modifies the morphology of newborn granule cells (18, 19), concomitant to hippocampus-dependent memory deficits, suggesting a role of hippocampal neurogenesis in post-stroke cognitive impairment. Furthermore, higher levels of hippocampal neurogenesis promote forgetting of old memories, which are otherwise strengthened by reducing neurogenesis (9, 20). We therefore explored hippocampus-dependent cognitive function as well as hippocampal neurogenesis and circuitry remodelling response after stroke and

examined whether neurogenesis modulation might ameliorate hippocampus-dependent cognitive function.

## RESULTS

### Cortical ischemia induces long-term hippocampus-dependent cognitive impairment

We first evaluated how permanent cerebral ischemia affects the formation of enduring memories using the contextual fear conditioning (Figure 1A-C). Seven days after surgery, sham and ischemic mice were placed in a chamber (context); after a familiarization phase, several electrical foot-shocks were presented, and recent and remote memory (24h, 28d or 60d after conditioning) was calculated by measuring the freezing response. Sham and ischemic mice behaved similarly during the training phase, displaying comparable exploratory activity and foot-shock reactivity (Suppl. figure 1A-B; $p>0.05$). In addition, the formation of new memories was not affected by middle cerebral artery occlusion (MCAO) since both sham and MCAO mice displayed similar conditioned response 1h after training (Suppl. figure 1C; $p>0.05$).

During the retention session, although sham and MCAO groups did not show any differences when tested 24h after training (Suppl. figure 1D; $p>0.05$), ischemic mice displayed decreased retrieval compared to sham group when remote memory was evaluated 28d later (Figure 1B; $p<0.05$ vs. sham). Importantly, this effect persisted at least 60 days after surgery (Figure 1C; $p<0.05$ vs. sham).

The degree of memory retention could be modulated by modifying the initial memory strength by using a weak or a strong contextual fear training paradigm (Figure 1D-F): while ischemic mice displayed less freezing behaviour than the sham group 28d after foot-shock presentation when using a weak fear conditioning protocol (Figure 1E, $p<0.05$ vs. sham), differences between sham and MCAO were abolished by a strong fear protocol (Figure 1E; $p>0.05$ vs. sham). Importantly, even with the latter, ischemic mice presented a low ratio of memory persistence when evaluated 60 days after training (Figure 1F; $p<0.05$ vs. sham), probably indicating a progressive cognitive decline which mimics that observed in stroke patients (3). We next asked whether the timing of new memory acquisition impacts long-term memory retention, and if the long-term memory

deficits dissipate with time. Of note, when conditioning was performed either 48h before surgery (Figure 1G; $p<0.05$ vs. sham), or 35 days after MCAO (Figure 1H; $p<0.05$ vs. sham), similar results were observed, indicating that cerebral ischemia impairs the recall of remote memories independently of the time at which that memory was formed (i.e., before, early after or even later after stroke).

Memory deficits after stroke are considered to be size and location-dependent (for rev., see 21). In our model, in which lesion is restricted just to the cortex and the initial and final lesion are directly correlated (Suppl. figure 2A, $p<0.05$), we did not detect any association between damage and degree of cognitive function, determined as freezing response (Suppl. figure 2B; $p>0.05$). Likewise, similar infarct volumes were observed along the antero-posterior axis (Suppl. figure 2C), with an exclusive cortical affectation, discarding that memory deficits were causally related to infarct size or location.

Enduring contextual fear conditioning memories have been ascribed to the hippocampus (22). To check whether cognitive impairment was due to the specific involvement of hippocampus, we examined the ability of retrieval of remote memories after hippocampal inactivation in both sham and ischemic mice (Figure 2A). First, 7 days after the surgery, mice were trained in contextual fear conditioning and tested 28d after. Twenty-four hours later, mice received a bilateral infusion of vehicle or tetrodotoxin (TTX) in the dorsal hippocampus and the freezing response was re-assessed 3h later. TTX administration in both sham and MCAO groups impaired retrieval compared to the vehicle-treated group, indicating that memory recall after fear conditioning in both groups is allocated to the hippocampus (Figure 2A; $p<0.05$ vs. sham).

Accordingly, an altered pattern of hippocampal c-Fos expression was observed in ischemic mice after the retrieval of long-term contextual fear conditioning (Figure 2B). While 90 min after the retrieval session, conditioned sham mice displayed an increase in the percentage of c-Fos$^+$ cells in different hippocampal subfields, CA1, CA3 and dentate gyrus (DG), relative to the unconditioned sham group (mice which were exposed to the

context during the retrieval session but did not receive any foot-shock 28d before), the population of hippocampal neurons activated by context re-exposure in ischemic mice was smaller in both ipsi- and contralesional hippocampus compared to sham group (Figure 2B; c-Fos$^+$ cells vs. unconditioned mice: sham: 3.79±0.43; MCAO ipsilesional: 1.59±0.29; MCAO contralesional: 1.51±0.36, n=6-7 mice/group; sham vs. MCAO ipsilesional, p=0.012; sham vs. MCAO contralesional, p=0.033), reinforcing the implication of the hippocampus in MCAO-induced retrieval impairment.

Finally, we explored whether ischemia could also affect other types of hippocampus-dependent memory such as spatial memory (Figure 2C-F). Seven days after surgery, mice were trained during 6 consecutive days (3 rounds/day) in the Barnes maze platform and, 28 days later, a probe trial was conducted without the escape box to measure spatial memory retention. Both sham and ischemic mice displayed similar speed and travelled distance and learned similarly to locate the escape hole with the hidden box during the course of the training period, as indicated by a progressive reduction in the time needed to reach the target hole (Suppl. figure 3A-D). However, confirming our previous results, ischemic mice displayed a decrease in spatial memory retention 28 days after training compared to the sham group, when estimated either as the time spent in the target quadrant (Figure 2E; $p<0.05$ vs. sham TQ) or as the time spent around the target hole (Figure 2F; $p<0.05$ vs. sham). All these data suggest that cortical stroke in mice promotes a long-term hippocampus-dependent cognitive impairment.

**Stroke-induced neurogenesis in the subgranular zone positively correlates with memory impairment after cerebral ischemia**

Cortical focal ischemia produces a long-term memory impairment which seems to be due to hippocampal affectation. Although no changes were found in overall hippocampal morphology or volume either 1 or 2 months after ischemia using Nissl staining or MRI, respectively (Suppl. figure 4A-D; $p>0.05$), MCAO mice presented a

significant increase in DG granular cell layer (GCL) volume compared to sham group 35d after surgery (Figure 3A-B; $p<0.05$ vs. sham). Interestingly, a negative relationship between GCL volume and freezing response was found in the ischemic group (Figure 3C; $r=-0.4972$, $p=0.0016$) indicating that animals with higher volumes displayed more severe cognitive deficits at the time studied.

In the SGZ of the DG, new granular neurons are generated throughout life. These newborn neurons integrate into hippocampal circuits playing a role in memory storage (23-25). Acute brain injury stimulates hippocampal neurogenesis in different experimental models but this response might have detrimental consequences and promote hippocampal malfunction, as observed in different pathologies such as epilepsy or schizophrenia (8). Increased SGZ neurogenesis has also been found in different cortical stroke models (26, 27). Since perturbations in neurogenesis may alter GCL/DG size, we reasoned that post-stroke neurogenesis could be involved in memory impairment observed after stroke. In our MCAO model (Figure 3D), an almost two-fold increase in the number of proliferating $Ki67^+$ cells and immature $DCX^+$ neurons were found in both ipsi- and contralesional SGZ 14 days after injury, which persisted at least 21 and 35d after ischemia, respectively (Figure 3E-H; $p<0.05$ vs. sham). Importantly, we found an inverse correlation between the numbers of $DCX^+$ cells and the freezing response, indicating that increased neurogenesis after cerebral ischemia leads to more severe cognitive deficits (Figure 3I; Spearman $r=-0.651$, $p<0.0001$). Accordingly, a positive correlation was found between GCL volume and $DCX^+$ cell number in the SGZ of ischemic mice (Figure 3J; Spearman $r=0.4177$, $p=0.0059$). We did not detect any differences between sham and MCAO groups in the numbers of cleaved-caspase $3^+$ cells (data not shown), but we observed an approximately 1.5-fold increase in the number of new neurons ($BrdU^+/NeuN^+$ cells) in both ipsi- and contralesional hippocampus 65d after ischemia (Suppl. figure 5A-D; $p<0.05$ vs. sham; sham: 503.61±33.40 cells; MCAO ipsilesional: 766.52±38.33 cells; MCAO contralesional: 723.34±34.57 cells), indicating that the increase in $DCX^+$ cells and the associated

cognitive deficits were not due to a higher death rate of newborn neurons. In addition, the increase in $DCX^+$ cells did neither correlate with lesion size (Suppl. figure 6A-B; $p>0.05$ vs. sham) nor with reductions in the number of postnatal generated neurons as consequence of ischemic stroke (Suppl. figure 7).

**Enhancement of post-stroke neurogenesis exacerbates hippocampal cognitive deficits after ischemia**

All these data suggest that levels of neurogenesis and memory deficits after ischemic injury are directly related. To reinforce this correlation, we tested whether interventions directed to further enhance SGZ neurogenesis could exacerbate cognitive deficits in the MCAO group (Figure 4). First, 7 days after surgery, we enhanced neurogenesis in both sham and MCAO mice by allowing them free access to a running wheel, while control animals remain sedentary with a locked running wheel in their home cages. Twenty-eight days later, running efficiently increased the number of both proliferating $Ki67^+$ cells (Figure 4A-B, $p<0.05$ vs. MCAO sedentary) and $DCX^+$ cells (Figure 4C-D, $p<0.05$ vs. MCAO sedentary) in both sham and MCAO groups compared to sedentary controls (Figure 4A-D and Suppl. fig 8A-B). To check whether over-stimulated neurogenesis after stroke exacerbates cognitive impairment, we evaluated memory retention after contextual fear conditioning (CFC; Figure 4E). Consistent with our hypothesis, 28 days after conditioning, running further impaired the recall of remote contextual fear memories relative to the sedentary groups (Figure 4E and Suppl. figure 8C; $p<0.05$ vs. sham or MCAO sedentary). In addition, MCAO impaired incidental context learning (Suppl. fig 8D, $p<0.05$ vs. sham), an effect that was further increased by running (Suppl. Fig 8D, $p<0.05$ vs. MCAO sedentary).

We next used the Barnes maze to determine if a comparable effect was also found in spatial memory (Figure 4F-I). Indeed, spatial memory deficits observed in the MCAO sedentary group were exacerbated in runner ischemic mice (Fig 4H-I), which did neither discriminate the target quadrant (Figure 4H, $p<0.05$ vs. MCAO sedentary) nor

the right hole (Figure 4I, $p<0.05$ vs. MCAO sedentary), showing a random behaviour with no preference toward any region of the Barnes maze.

To reinforce our results, we next asked whether analogous memory deficits would be observed by using memantine (MEM; Figure 4J-L), as a pharmacological approach to increase neurogenesis after stroke injury (28). Consistent with our previous results, MEM treatment increased post-stroke SGZ neurogenesis, estimated as an increase in the number of $DCX^+$ cells (Figure 4J-K and Suppl. figure 9A; $p<0.05$ vs. MCAO vehicle) while impairing remote memory recall as demonstrated by a decreased freezing response (Figure 4L and Suppl. figure 9B; $p<0.05$ vs. MCAO vehicle). All these data support that enhanced hippocampal neurogenesis negatively interferes with the retrieval of memories and could therefore contribute to cognitive deficits after stroke.

**Stroke-induced newborn neurons promote differential hippocampal circuitry remodelling**

Memory retrieval may result from the reactivation of the same neuronal ensembles at the time of memory encoding (29, 30). Enhanced integration of newborn neurons into hippocampal circuits due to high neurogenesis levels could negatively regulate the ability to recall memories by replacing pre-existing synapses and therefore remodelling hippocampal connections where memory is stored, a mechanism that has been demonstrated to mediate forgetting (9). This mechanism might thus explain the inverse correlation found between neurogenesis and hippocampal performance in our cortical ischemia model. However, in our scenario, an alternative and/or additional explanation might be the presence of pathological neurogenesis. Indeed, aberrant morphological alterations have been described for SGZ newborn neurons after MCAO (18, 19). To gain further insight into the mechanisms which contribute to cognitive impairment in our cortical stroke model, we characterized the distribution of the dendritic arborisation along granular and molecular layers in immature neurons ($DCX^+$; Suppl. figure 10A-D). Of note, differential patterns were found for ipsi- and contralesional DGs.

While a clear increase in the % of dendritic arborisation in the molecular layer (ML) was observed for the contralesional hippocampus, no significant differences were detected for the ipsilesional side (Suppl. figure 10A and C; $p<0.05$ vs. sham and MCAO ipsilesional ML1, respectively). Interestingly, differential results were also found in the number of immature large mossy fibres terminals (LMTs-$DCX^+$) reaching the CA3 region. Whereas a reduction in the number of LMTs in CA3 was detected in the ipsilesional side, on the opposite, an increased synaptic rearrangement was found in the contralesional CA3 (Suppl. figure 10B, D-E; $p<0.05$ vs. sham and MCAO ipsilesional, respectively), further suggesting that differential remodelling processes are taking place in parallel at the ipsi- vs. the contralesional hippocampus after ischemia.

To confirm these results, 14 days after surgery we infused GFP-expressing retrovirus into the DG of sham and ischemic mice in order to evaluate newborn neuron integration and possible circuit remodelling (Figure 5A-B). Sholl analyses revealed a comparable phenotype to that observed for $DCX^+$ arborisation in contralesional DG $GFP^+$ neurons, corroborating an increase in dendritic branching in the distal segment (150-250 µm from the soma; Figure 5C-D; $p<0.05$ vs. sham and MCAO ipsilesional, respectively) and in total dendritic length (Figure 5E; $p<0.05$ vs. sham and MCAO ipsilesional, respectively). Remarkably, an opposite phenotype was found in ipsilesional ischemic $GFP^+$ newborn neurons, with an increased degree of branching in the proximal domain (0-50µm from the soma; Figure 5C-D; $p<0.05$ vs. sham and MCAO contralesional, respectively) and a retraction of the distal domain in the molecular layer (ML). Accordingly, ipsilesional $GFP^+$ neurons also displayed a reduction in total dendritic length (Figure 5E).

Mature granule newborn neurons generally display only one apical dendrite which remains almost no ramified until it reaches the ML where it begins to extend its branches and establishes synapses with afferents of the perforant pathway from the entorhinal cortex (EC). Therefore, apical dendrite growing seems to be a critical factor for the correct integration of newborn neurons (31, 32). Our data also demonstrate a

differential pattern of apical dendrite growth in $GFP^+$ neurons of the ipsi- vs. the contralesional ischemic DG. Contralesional ischemic $GFP^+$ neurons presented a longer apical dendrite compared to both ipsilesional and sham $GFP^+$ neurons (Figure 5F and Suppl. figure 11A). On the contrary, ipsilesional $GFP^+$ neurons showed a dramatic reduction in the apical dendrite length compared to the other groups (Figure 5F; $p<0.05$ vs. sham and MCAO contralesional, respectively). Interestingly, when we classified $GFP^+$ neurons in each group according to apical dendrite length intervals (Figure 5G and Suppl. figure 11A), our data demonstrate that apical dendrite growth alteration due to ischemic stroke differentially affects approximately 30% of the newborn neuron population in ipsi- (predominant aberrant phenotype <10μm) and contralesional sides (predominant aberrant phenotype 40-70μm), compared to the $GFP^+$ neurons observed in sham mice (predominant phenotype 10-40μm). We also analysed whether stroke affected spine density of $GFP^+$ newborn neurons as an index of synaptic integration. Of note, despite their altered dendrite arborisation, no differences were observed in the density of dendritic spines of $GFP^+$ newborn granule cells either in the ipsi- or in the contralesional side when compared to the sham group (Suppl. figure 11B-C), suggesting that these newborn neurons are integrated into hippocampal circuits receiving inputs from the EC.

As previously demonstrated for post-stroke neurogenesis, aberrant features of newborn neurons might be also transient after stroke. For assessing this issue, in a different set of experiments, the GFP-expressing retrovirus was delivered 35 days after stroke (Suppl. figure 12A), when post-stroke neurogenesis had already returned to physiological levels. Interestingly, although the aberrant features of newborn neurons previously detected in the Sholl analysis or in mean apical dendrite length were not observed at this time point (Suppl. figure 12B-C), 30.5% of the ipsilesional newborn population still displayed apical dendrite growth alterations (aberrant phenotype <10μm; Suppl. figure 12D-E), an effect that might lead to an incorrect integration of axonal projections coming from entorhinal cortex.

All these results indicate that ischemic stroke promotes an increase in neurogenesis that gives rise to the generation of differential populations of newborn neurons with altered morphological features depending on their ipsi- or contralesional location, an effect which remains, at a significantly lower intensity, when the levels of neurogenesis become normalised. Altogether, the integration of these abnormal neurons could promote aberrant hippocampal circuitry rearrangements and, therefore, contribute to hippocampal cognitive deficits observed after ischemia.

**Post-stroke memory impairment is reduced by down-regulation of aberrant-induced neurogenesis**

Our data support that high levels of post-stroke neurogenesis initiate a differential remodelling of hippocampal circuits which contributes to cognitive deficits after stroke. Therefore, we predicted that decreasing aberrant post-stroke neurogenesis towards physiological levels might ameliorate ischemia-induced hippocampal deficits. For this, we used both pharmacological and genetic strategies. First, we suppressed post-stroke neurogenesis by treating mice with temozolomide (TMZ), a DNA-alkylating agent (Figure 6 and Suppl. figure 13). TMZ treatment caused a reduction of neurogenesis in MCAO mice, as reflected by reduced numbers of proliferating $Ki67^+$ cells and immature neurons expressing DCX (Figure 6A-B; $p<0.05$ vs. MCAO vehicle, and Suppl. figure 13). Importantly, and confirming our hypothesis, TMZ treatment improved memory retrieval in parallel to a reduction in neurogenesis as shown by an increased freezing response in mice evaluated 28 days later (Figure 6C-D; $p<0.05$ vs. MCAO vehicle).

To reinforce our results, we genetically ablated aberrant hippocampus-generated neurons after ischemia by using Nestin-$Cre^{ERT2}$/NSE-DTA mice (33-35) (Figure 7A). After tamoxifen administration, a STOP region in the diphtheria toxin fragment A (DTA) cassette gene is deleted in $nestin^+$ neural stem cells (NSCs). These cells will die by apoptosis at the beginning of their neuronal differentiation, due to the DTA expression under the Eno2 (neuron-specific enolase 2) promoter gene. Genetic ablation of newly

formed neurons after stroke led to a decrease in $DCX^+$ cells (Figure 7B-C; $p<0.05$ vs. Nestin-$Cre^{ERT2}$/NSE-DTA vehicle, and Suppl. figure 14A-B) in parallel to a better performance in both contextual fear (Figure 7D, $p<0.05$ vs Nestin-$Cre^{ERT2}$/NSE-DTA vehicle, and Suppl. figure 14C) and Barnes maze test (Figure 7E-H, $p<0.05$ vs. Nestin$Cre^{ERT2}$/NSE-DTA vehicle).

Altogether, our data demonstrate that the increased levels of post-stroke neurogenesis contribute to cognitive hippocampal deficits observed following injury, very likely by producing an aberrant remodelling of hippocampal circuits.

## DISCUSSION

Ischemic stroke is considered one of the most disabling illnesses in our days (1). Most of the studies in this field have been focused on strategies to limit the expansion of the initial damage as well as the motor effects (2). However, clinical-pathological studies have revealed stroke as a major contributor to cognitive impairment in patients (rev. in 5, 36, 37). Due to the heterogeneity of the mechanisms underlying cognitive deficits and the lack of effective animal models to recapitulate this condition, the pathophysiological knowledge and the development of treatments for post-stroke cognitive impairment remain an urging therapeutic challenge. In the present study, we have investigated the mechanisms underlying long-term memory deficits driven by cortical ischemic stroke. Through a series of studies, we show that cortical ischemia in mice promotes memory impairment due, at least partly, to a pathological hippocampal circuitry remodelling prompted by the post-stroke hippocampal neurogenic response.

First, in our cortical stroke model, we observed a long- but not short-term impairment in both episodic and spatial memories after ischemic stroke supporting that, after this type of acute damage, there is a progressive and persistent decline of cognitive functions which resembles that observed in stroke patients (2, 3, 5, 10, 36). The impairment was independent of whether the memory was formed before, early after, or even long-term after stroke, at least for the times and conditioning protocols tested in this study. The risk to develop post-stroke cognitive impairment has been associated with the extent of lesion size and its strategic location (37). In order to study the mechanisms associated with a specific location, we took advantage of the low degree of variability and the cortical location of our stroke model, which allowed us to discard brain structural alterations located outside of the cortical ischemic lesion and that could also participate in the observed cognitive impairment.

In the adult mammal brain, the hippocampus is one of the main regions implicated in cognitive functions. Importantly, although our MCAO model neither directly affects the overall hippocampal anatomy nor causes a secondary long-term atrophy, we have

confirmed the implication of this structure by different approaches. First, hippocampus inactivation by TTX infusion completely abolished the ability of retrieval in both MCAO and sham groups, indicating that a correct activation of this structure is critical to bring the memory back after our stroke model. Second, stroke hindered the proper activation of hippocampus to recall old memories, determined as a reduction in the number of hippocampal c-Fos$^+$ cells after long-term retrieval. All these results point to the hippocampus as the main contributor for post-stroke memory impairment in our cortical ischemia model.

Adult hippocampal neurogenesis occurs in SGZ of the DG, which is considered a source of new neurons that persists in the adult hippocampus of most mammals, including humans (8, 38, 39). Thus, newborn neurons are continually being generated providing new potential substrates for the incoming information (40-43). Importantly, numerous examples have been provided for the role of physiological and pathological neurogenesis in hippocampus-dependent learning and memory processes (10, 11, 44). Using a long-term temporal study, we hereby describe a longitudinal profile of the neurogenic response in both ipsi- and contralesional SGZ during the chronic phase of stroke. Specifically, we have observed an increased number of proliferative cells, two weeks after stroke onset, and of immature newborn neurons (neuroblasts) which remained enhanced 1 month after the ischemic injury. This neurogenic response could account for the augmentation of the GCL volume since the majority of stroke-induced DCX$^+$ cells were finally fully integrated into the hippocampal circuits at the time studied. Interestingly, an inverse correlation was found between neurogenesis levels and memory recall, supporting that higher levels of SGZ neurogenesis are a modulating factor of cognitive performance that may contribute to impaired memory retrieval after stroke. This idea was reinforced by the results obtained after enhancing post-stroke neurogenesis by physical activity or by a pharmacological approach using memantine (25, 28), showing a more severe cognitive decline in contextual and spatial memory after ischemia.

Whereas the addition of newborn cells in the DG provides new potential sources for storing incoming information, the integration of newborn neurons may also promote a remodelling of circuits where memory is stored, weakening existing memories, a phenomenon known as “forgetting” (9, 45). This body of evidence implies that, due to the net increase in newborn neurons after stroke, remodelling of hippocampal circuits could drive the forgetting of previously acquired information. The vast majority of cells generated in the SGZ differentiate into dentate granule cells, extending 1) their apical dendrite towards the molecular layer where it extensively ramifies, and 2) their axons, called large mossy fibre terminals, towards targets in CA3 region, forming input and output synaptic connections (17, 40, 46). However, after stroke, newborn neurons display different morphological alterations that might hinder their proper integration into the hippocampal circuits (19). Importantly, our results show a different remodelling process occurring simultaneously at each side of the hippocampus after ischemic stroke, demonstrated by distinctive morphological alterations observed in newborn neurons at the ipsi- and contralesional hippocampi. Indeed, by analysing immature and mature newborn neurons, our results are the first demonstration of a different phenotype of newborn neurons at the ipsilesional when compared with contralesional hippocampus which seems to affect both synaptic inputs and outputs, beyond the physiological “forgetting” induced by enhanced neurogenesis. On one hand, one important difference between phenotypes is the different pattern of dendritic arborisation probably driven by a differential apical dendrite growth. Whereas ipsilesional ischemic neurons show an increased proximal dendritic branch density, contralesional neurons display an elongation of apical dendrite and, consequently, an increase in distal dendrite branch. This altered dendritic branching could have important consequences for incoming information from the EC, since inputs in the inner and outer molecular layers carry different information (47) and, thus, could have profound functional implications at the network level. On the other hand, our data suggest that stroke also promotes a differential bilateral remodelling in the connectivity between DG and CA3. Each new cell

in the DG projects a mossy fibre that reaches the CA3 region within approximately 2 weeks, contacting with 11–15 pyramidal cells (40, 42, 48). Interestingly, in CA3, we report a hyper- or a hypointegration pattern of immature newborn neurons at the contra- and ipsilesional hemisphere, respectively. These data could imply an increased synaptic rearrangement in the contralesional CA3, which could co-exist or replace the previous DG-CA3 synapses. Although we have not confirmed this result in full mature neurons, newly generated neurons transiently (2-6 weeks of the cell age) display enhanced synaptic plasticity (49, 50), suggesting that these immature new neurons may also transiently have the ability to deprive pre-existing synapses and, therefore, contribute to deficits observed in our model.

The transient nature of post-stroke induced neurogenesis suggests that the production of abnormal newborn granule neurons could also be temporary. Indeed, we have observed that aberrant features of newborn neurons decrease at later times after stroke, in agreement with a return of neurogenesis to basal levels; however, our data show that the generation of aberrant newborn neurons, although at a significantly lower extent, persists at later times suggesting that the factors that induce morphological remodelling, albeit likely decreasing along time, are still present at later time points. This is to be added to the important fraction of aberrant neurons generated during the stroke-induced neurogenic burst which will likely remain abnormally integrated into the hippocampal circuits. All together, they are likely to contribute to the persistent cognitive deficits found at the latest time points studied.

As commented above, when testing hippocampus-dependent memory in a retrograde fashion, increasing neurogenesis after memory acquisition induces “forgetting” due to the interference caused by the integration of newborn neurons within the pre-existing hippocampal circuits (9). However, the generation of new mature granule neurons in the hippocampus has been traditionally thought to be an endogenous mechanism for cognitive repair, in agreement with a positive effect of neurogenesis on anterograde memories by which new neurons synaptically integrate into hippocampal

circuits offering a substrate for acquisition of new memories (learning). In the context of cerebral ischemia, a substantial amount of evidence supports a positive role of neurogenesis in stroke models. Of note, in most models used, the injury affects directly the hippocampus, as after global ischemia (51, 52) or after models of focal ischemia with hippocampal affectation (15, 53, 54). In similar settings, physical exercise, an intervention known to increase neurogenesis, has been shown to promote neurocognitive recovery in rodents (rev. in 8, 55). However, in these studies, basal affectation of hippocampus caused by a direct ischemic injury is likely to explain the positive effect of neurogenesis. It should be noted that some studies have reported positive effects of neurogenesis on cognitive function in stroke models without hippocampal affectation. For instance, hypoxic postconditioning stimuli increased neurogenesis in parallel to a better cognitive performance (56); however, in this case, abolition of neurogenesis did not affect cognitive function in MCAO-exposed rats. In this line, genetic abolition of neurogenesis has been described to worsen cognitive function after stroke (17); nevertheless, neurogenesis ablation was performed prior to the MCAO procedure, a reason for which those mice are likely to display a basal cognitive deficit, on which the effects of neurogenesis, as in the damaged hippocampus, are likely to be beneficial. Therefore, the positive effect of neurogenesis on anterograde memories after stroke, including when physical exercise interventions are tested, is demonstrated when the hippocampus shows some degree of affectation, a situation which does not correspond with our experimental setting in which the hippocampus remains intact after the MCAO. In contrast, and similarly to our results, other studies have observed the detrimental effect of stroke in the morphological features and correct integration of newborn granule cells, in parallel to impaired spatial memory (18, 19).

Apart from physical exercise interventions, pharmacological tools such as memantine and fluoxetine have been described to be useful to increase neurogenesis (28, 57). By this mechanism, memantine has been shown to exert a negative effect on retrograde memories (“forgetting”) (9, 58). This might seem conflictive with the current

clinical use of this drug, which is the treatment of moderate to severe Alzheimer's disease (AD). However, the well-known action of memantine as a non-competitive, low- to medium-affinity antagonist of brain NMDA glutamate receptors is likely the major mechanism that accounts for its beneficial effect in AD.

Our data suggest that an aberrant hippocampal circuitry remodelling due to stroke-induced neurogenic response could explain, at least partly, post-stroke cognitive impairment. To confirm our hypothesis, we abolished stroke-induced neurogenesis using pharmacological (TMZ) or genetic approaches (Nestin-Cre$^{ERT2}$/NSE-DTA mice). With both approaches, stroke-induced increase in neurogenesis was ablated, as shown by a return to basal levels in numbers of both proliferating cells and immature newborn neurons at the DG. Remarkably, a major result of our present work is that, after these strategies, MCAO mice displayed an improvement in contextual and spatial memory recall performance, supporting the important role of stroke-induced neurogenesis in cognitive impairment. Considered as a pathological response, we are the first to propose the inhibition of aberrant hippocampal post-stroke neurogenesis with the aim to avoid the onset of long-term memory deficits after stroke.

Several mechanisms could account for post-stroke aberrant neurogenesis. On one hand, mediators of post-ischemic excitotoxicity or cortical spreading depression, such as $K^+$ and glutamate elevations, could be involved as both have been implicated in an enhanced proliferation of immature cells while at the same time directing toxicity in more mature cell types (59, 60). Another influence to be considered is the inflammatory response elicited by the injured brain, whereby astrocytes and microglia activation could lead to the secretion of a variety of growth factors and immune modulators able to affect progenitor proliferation and survival (61, 62). In addition, injury-induced circulating factors might affect directly neural progenitors which are in physical contact with the vasculature (63).

Overall, our results identify hippocampal circuitry remodelling after stroke-induced neurogenesis response as a new process that promotes the loss of

hippocampus-dependent memories. We show that stroke-induced neurogenesis could be considered as a therapeutic target for the treatment of the cognitive decline shown by stroke patients, opening new lines of research in the development of new treatments for this devastating condition.

## METHODS

### Animals

Experiments were performed in male C57Bl/6 mice of 8-10 weeks obtained from The Jackson Laboratories. NSE-DTA mice (Eno2-Stop-DTA mice) were kindly donated by from Prof. S. Itohara and Prof. Y. Kobayashi (RIKEN Center for Brain Science, Saitama Japan; 34, 35) and were maintained through homozygous breeding pairs. Nestin-Cre$^{ERT2}$/NSE-DTA mice were generated by crossing NSE-DTA mice with Nestin-Cre$^{ERT2}$ mice (33) and then maintained through homozygous breeding pairs on a C57BL/6 background. In these transgenic mice (Nestin-CreERT2/NSE-DTA), tamoxifen-inducible Cre is expressed by neural stem cells under the nestin promoter and the loxP-STOP-loxP-IRES-diphtheria toxin fragment A (DTA) gene cassette is knocked into the neuron-specific enolase (NSE, Eno2) gene. After tamoxifen treatment, Cre recombinase deletes the STOP sequence in the neural stem cell pool. Throughout the maturation, NSE promoter becomes active inducing the expression of DTA resulting in a cellular programmed death. Thus, the generation of fully mature newborn granule neurons is dramatically decreased in those mice. The following primers were used for genotyping Nestin-CreERT2 mice: 5´- TTCCGCTGGGTCACTGTCGCCGCTAC-3´ and 5´-TAATCGCGAACATCTTCAGGTTCTGC-3´; for NSE-DTA mice: 5´-AATTCTTAATTAAGGCGCGCCGG-3´, 5´-GTCAGAATTGAGGAAGAGCTGGGG-3´and 5´-CACTGAGGATTCTTCTGTGG-3´.

Animals were kept in a room with controlled temperature and a 12-hour dark/light cycle and fed with standard food and water *ad libitum*.

All the experiments display biologically independent samples except for animals shown in Figure 1B, which were used for the correlations shown in Figure 3, for Suppl. figs. 2A-C and for Suppl. figure 4B, and animals for sham and MCAO control groups, which were used for testing the effect of running and temozolomide on both neurogenesis levels and CFC memory in Figs. 4 and 6, and Suppl. figs. 8 and 13.

**Middle cerebral artery occlusion (MCAO) in mice**

Mice were subjected to permanent focal cerebral ischemia through the distal occlusion of MCA (middle cerebral artery) as previously described (64). Briefly, mice were anesthetized with isoflurane 1.5-2% in a mixture of 80% air-20% oxygen, and body temperature was maintained at physiological levels with a heating pad during the surgical procedure and anaesthesia recovery. Mice were subjected to permanent focal cerebral ischemia (MCAO) through the distal occlusion of MCA by ligature of the trunk just before its bifurcation between the frontal and parietal branches with a 9-0 suture, in combination with the occlusion of the ipsilesional common carotid artery. Mice in which the MCA was exposed but not occluded served as sham-operated controls (sham). Following surgery, individual animals were returned to their home cages with free access to water and food. All the groups were performed and quantified in a randomized fashion by investigators blinded to treatment groups.

**Infarct volume measurement**

Infarct size was determined by magnetic resonance imaging 24-48 hours after MCAO using a BIOSPEC BMT 47/40 (Bruker, Ettlingen, Germany). Infarct volume was calculated using the ImageJ software (NIH, USA) from the T2-weighted images as described (65). In addition, infarct size was determined by Nissl staining as described (64).

**Determination of hippocampus and dentate gyrus (DG) volume**

The volume of the hippocampus and the DG was estimated stereologically by applying the Cavalieri method, performed with Stereo Investigator software (MicroBrightField, Williston, VT) to each series of Nissl-stained sections. Volumes were estimated by using a one-in-five systematic random series of 30-μm Nissl-stained using a 100 and 20-$\mu m^2$ point-counting grid, respectively.

**Treatments**

*Running*: Mice in running groups (3 mice/cage) were given voluntary access to 2 running wheels placed in their home cages. Access to wheels started 7 (CFC) or 12 days (Barnes maze) after ischemia and 24 hours post-training. Sedentary controls were similarly housed but running wheels were locked during all the procedure.

*Tamoxifen*: Nestin-Cre$^{ERT2}$/NSE-DTA mice were injected intraperitoneally daily with tamoxifen (150mg/Kg) in sunflower oil for 5 consecutive days starting 7 days after ischemia and 24 hours post-training.

*BrdU*: For experiments aimed to study the number of newborn granule neurons 65 days after MCAO, BrdU was dissolved in phosphate-buffered saline (PBS) and injected in 2 rounds of treatment at 1-week intervals, with each round consisting of one injection (100 mg/kg, i.p.) per day for 5 consecutive days and starting 10 days after ischemia. For post-natal labelling, BrdU was administered for 5 consecutive days, one injection (100 mg/kg, i.p.) per day and starting when mice were 1-month-old.

*Memantine*: Mice were administered memantine (MEM; 0.9% saline, 25 mg/kg, i.p.) once per week during 4 weeks as previously described (58). MEM administration started 7 days after ischemia and 24 hours post-training.

*Temozolomide*: Mice were given four rounds of treatment at 1 week intervals, with each round consisting of one injection of temozolomide (TMZ; 0.9% in saline containing 10% DMSO, 25 mg/kg, i.p.) per day for 4 consecutive days (66). TMZ administration started 7 days after ischemia and 24 hours post-training.

*Tetrodotoxin*: Hippocampus activity was transiently inactivated by infusion of tetrodotoxin (TTX, a sodium channel blocker) (67). Three hours before the retrieval session, mice received an infusion of 0.5 µl of TTX (20 µM, Wako, Neuss, Germany) at a rate of 0.2 µl/min into the hippocampus (-2 mm AP, -1.7 mm ML relative to bregma, and -2 mm DV from skull) with a 5-µl 32s-gauge Hamilton syringe.

*Retrovirus*: New neurons were labelled using a murine Moloney leukemia virus-based retroviral vector (CAG-GFP, Addgene, Teddington, UK; 40). Concentrated viral solutions were prepared by transfection of retroviral vectors into Gryphon Eco cells, followed by ultracentrifugation of viral supernatant and concentrated virus solution by ultra-speed centrifugation ($10^{8-9}$u/ml). Mice were anesthetized with isoflurane and placed in a stereotaxic frame.

Two µl of retrovirus were infused at a rate of 0.2 µl/min into the DG (-2 mm AP, -1.4 mm ML relative to bregma, and -2.4 mm DV from skull) with a 5-µl 32s-gauge Hamilton syringe. Retroviral injections were performed 14 or 35 days after surgery in both sham and MCAO groups and morphological analysis were performed 28 days later.

**Behavioural testing**

*Contextual Fear Conditioning (CFC)*: CFC occurred in test chambers (31 cm x 24 cm x 21 cm) with shock-grid floors (bars 3.2 mm in diameter spaced 7.9 mm apart). The front, top and back of the chamber were clear acrylic and the sides were modular aluminium. Contextual fear conditioning was performed 7 days after surgery in both sham and MCAO groups except for a set of experiments in which conditioning was performed 48h before surgery or 30 days after surgery. During conditioning, mice were placed in the chamber and, after 150 s of familiarization, they received three foot-shocks (0.6 mA, 2 s duration, 1 min apart). Mice were removed from the chamber 1 min after the last shock. In an additional set of experiments, a weak (0.4 mA x 2, 2 s duration, 1 min apart) or a strong (0.8 mA x5, 2 s duration, 1 min apart) conditioning protocol was also used. During the retrieval test, mice were placed in the chamber for 5 min. Behaviour was recorded by overhead cameras. Freezing (i.e. absence of movement except for breathing) was measured using automated scoring system for mice. In addition, activity, inactivity and grooming were also measured.

*Incidental Context Learning*: Incidental context learning in mice occurred in the same chambers as described above. During the context pre-exposure session (performed 7

days after surgery), mice were placed in the chambers for 10 min. During the immediate shock session, mice were returned to the chambers, a single foot-shock was immediately delivered (≤ 1 s after entry, 1 mA, 2 s duration), and mice were removed from the chambers after 1 min. During the retrieval session (24h later), mice were placed in the chambers for 5 min.

*Barnes maze*: A white circular platform (100-cm diameter, 70 cm above the floor) contained 20 holes equally spaced around its perimeter. Under one of the holes there was a black Plexiglas escape box (17 x 13 x 7 cm) filled with paper bedding. The location of this escape hole was always in the same place for all mice. For avoiding navigation based on olfactory or proximal cues within the maze, the platform was rotated before each trial, and the spatial location of the escape hole remained in a fixed location with respect to the distal room cues. During habituation, mice were allowed 5 min to freely explore the maze, with no escape box present. During training, mice were given 3 trials per day for 7 consecutive days. On each trial, mice were released in the centre of the maze and allowed 10 min to enter the escape box, where they remained for 30 s. If a mouse failed to find the escape box, it was guided by the experimenter. During the retrieval test, the escape box was removed from the maze, and mice were allowed to search for 3 min. Behaviour was recorded by overhead cameras and tracked using automated *Ethowatcher* software (UFSC, Florianopolis, Brazil). Time spent around each hole and arounds each quadrant was measured.

**Histology**

*Tissue preparation.* Mice were perfused transcardially with phosphate buffer (0.1M) followed by 4% paraformaldehyde (PFA). Brains were post-fixed in PFA and transferred to 30% sucrose. Coronal sections (30µm) were cut using a microtome (Leica SM2000R) and stored in cryoprotective solution.

*Nissl staining*. Brain tissue sections were placed in 0.5% cresyl violet in distilled water for 10 min at room temperature. Briefly, sections were rinsed in 75%, 90 and 100%

ethanol twice for 5 min before being dehydrated in xylene three times for 5 min. Sections were mounted with Permount.

*Immunohistochemistry*. Immunofluorescence was performed on free-floating sections that were incubated overnight at 4ºC with the following primary antibodies: goat anti-calbindin (1:500, SantaCruz Biotechnology, Heidelberg, Germany, ref. sc-7691), mouse anti-NeuN (1:500, Merck, Darmstadt, Germany, ref. MAB377), goat anti-doublecortin (DCX) (1:500, SantaCruz Biotechnology, Heidelberg, Germany, ref. sc-8066), rabbit anti-DCX (1:500, Abcam, Cambridge, UK, ref. ab18723), rabbit anti-c-Fos (1:1000, Abcam, Cambridge, UK, ref. 7963, and Merck, Darmstadt, Germany, ref. PC05L), rabbit anti-mouse Ki67 (1:500, Abcam, Cambridge, UK, ref. ab137876), chicken anti-GFP (1:700, ThermoFisher Scientific, Waltham, MA, USA, ref. A10262) and goat anti-Znt3 (1:3000, SantaCruz Biotechnology, Heidelberg, Germany, ref. sc-27508). For BrdU staining, free-floating sections were pre-treated with 2N HCl for 30 minutes at 37ºC and then incubated overnight at 4ºC with rat anti-5-bromo-2'-deoxyuridine (BrdU; 1:500, AbD Serotec, Kidlington, UK; ref. 0BT0030S). For cleaved caspase 3 staining, sections were pre-treated with 0.01M citrate buffer (pH 6.0) in a 97º C steamer for 15 min and allowed to cool to room temperature for 20 min and then incubated overnight with rabbit anti-cleaved caspase 3 (1:100, Cell Signalling Technology, Leiden, Netherlands, ref. 9661S). The secondary antibodies used were donkey Alexa-488 anti-goat (1:500, ThermoFisher Scientific, Waltham, MA, USA, ref. A11055), donkey Cy3 anti-mouse (1:500, Merck, Darmstadt, Germany; ref. AP192), goat Alexa-488 anti-chicken (1:500, ThermoFisher Scientific, Waltham, MA, USA, ref. A11039) and donkey Cy3 anti-rabbit (Merck, Darmstadt, Germany, ref. AP182C). Controls performed in parallel without primary antibodies showed very low levels of nonspecific staining.

*Image acquisition, processing and quantification*. Acquisitions were performed with a laser-scanning confocal imaging system (Zeiss LSM710, Jena, Germany) and image analysis was carried out with the ZEN2009 (Zeiss) software. Image quantification was performed with ImageJ Software (NIH, USA). The number of $Ki67^{+}$ and doublecortin

(DCX) cells were counted in confocal z-stack images. For that, 4-8 serial sections (30 µm) per animal spaced 300 µm apart (from bregma -1.46 mm to bregma -2.30 mm) were used. $Ki67^+$ and $DCX^+$ cells were counted manually in frames of 212.55µm x 212.55µm (1024x1024). Data is expressed as the number of cells per section.

For assessing the number of newborn neurons in the hippocampus ($Brdu^+/NeuN^+$ or $BrdU^+/calbindin^+$ cells) and the number of c-Fos cells, ten hippocampal sections, sampled every 5th section (from bregma-1.46 mm to bregma -2.30 mm) were used. The total number of $BrdU^+$ in the DG was calculated by multiplying the count in each section by 10 and then totalling the values. The images were taken at 63x and colocalisation of NeuN or $calbindin^+$ with $BrdU^+$ was confirmed by orthogonal projection of z-stack files. $c\text{-}Fos^+$ cells were counted manually in different hippocampal regions (CA1, CA3 and DG), and total cell numbers were calculated by multiplying the count in each section by 10 and then totalling the values of all regions as the sum of CA1, CA3 and DG $c\text{-}Fos^+$ cells. $c\text{-}Fos^+$ cell numbers in the conditioned groups (both sham and MCAO) were expressed as a percentage relative to the untrained/unconditioned group (mice which were exposed to the context but did not receive any foot-shock).

For morphometric analysis, two series of 50-µm coronal sections from each animal were used for the immunohistochemical detection of GFP-labelled neurons. Confocal 40X stacks of images were obtained and z-projections were used to trace neurons using the NeuronJ plugin for ImageJ software. Sholl´s analysis was then performed in order to determine dendritic complexity (determination of total dendritic length, apical dendrite length and degree of dendritic arbour branching) using the plugin Sholl Analysis for ImageJ (68). This analysis consists of placing a central point on the cellular soma and tracing concentric circles with 10um of distance interval between them. Each intersection between dendritic branches and circles was represented (68). For spines analysis, images of GFP-labelled dendritic processes at the outer molecular layer were acquired at 0.5-µm intervals with a plan apochromatic 63x oil lens [numerical aperture (NA), 1.4] and a digital zoom of 3. The *lsm* images files were subjected to two

iterations of deconvolution with the AutoDeblur program (AutoQuant, Troy, NY, USA). The length of each dendritic segment was measured, and the number of spines was counted manually. Spine density was calculated by dividing the total number of spines by the length of the dendritic segment. For the quantification, 10-15 dendritic segments from each animal per group were used. Confocal imaging and data quantification were performed blinded to the experimental conditions.

**Statistical analysis**

The results are expressed as the mean ± S.E.M. for the indicated number of experiments and the statistical analyses were performed using Prism5 software (GraphPad Software, San Diego, CA, USA). Comparisons between 2 groups were performed using non-parametric Mann-Whitney test, while those involving >2 groups were performed using non-parametric one-way ANOVA or two-way ANOVA followed by Bonferroni post hoc testing. Correlation analyses were performed using Spearman's correlation. Differences were considered statistically significant at $p<0.05$.

**Study approval**

All the experimental protocols performed have been approved by the Animal Welfare Committee of the Universidad Complutense and the Regional Government of Madrid (following EU directives 86/609/CEE and 2003/65/CE, and Spanish directives RD53/2013).

## AUTHORS CONTRIBUTIONS

MIC, JdP and MAM designed the research studies; MIC, JdP, APR, VDL, IBF and AGC conducted the experiments and/or acquired the data; JD and PWF provided valuable reagents; MIC, JdP, JMGS, JD, PWF, IL and MAM contributed to the analysis and/or the interpretation of the results; MIC, JdP, IL and MAM wrote the manuscript, which all the authors reviewed and approved.


## ACKNOWLEDGMENTS

This work was supported by grants from Spanish MINECO (SAF2015-68632-R) to MAM, from Instituto de Salud Carlos III (ISCIII; FIS PI17/01601) and ISCIII cofinanced by Fondo Europeo de Desarrollo Regional (FEDER) “Una manera de hacer Europa” RETICS RD12/0014/0003 to IL, and from Canadian Institutes of Health Research (FDN143227) to PWF.

**REFERENCES**


1. Benjamin EJ, Blaha MJ, Chiuve SE, Cushman M, Das SR, Deo R, et al. Heart Disease and Stroke Statistics-2017 Update: A Report From the American Heart Association. *Circulation.* 2017;135(10):e146-e603.
2. Mijajlovic MD, Pavlovic A, Brainin M, Heiss WD, Quinn TJ, Ihle-Hansen HB, et al. Post-stroke dementia - a comprehensive review. *BMC Med.* 2017;15(1):11.
3. Levine DA, Galecki AT, Langa KM, Unverzagt FW, Kabeto MU, Giordani B, et al. Trajectory of Cognitive Decline After Incident Stroke. *JAMA.* 2015;314(1):41-51.
4. Brainin M, Tuomilehto J, Heiss WD, Bornstein NM, Bath PM, Teuschl Y, et al. Post-stroke cognitive decline: an update and perspectives for clinical research. *Eur J Neurol.* 2015;22(2):229-38, e13-6.
5. Pendlebury ST, and Rothwell PM. Prevalence, incidence, and factors associated with pre-stroke and post-stroke dementia: a systematic review and meta-analysis. *Lancet Neurol.* 2009;8(11):1006-18.
6. Tatemichi TK, Desmond DW, Stern Y, Paik M, Sano M, and Bagiella E. Cognitive impairment after stroke: frequency, patterns, and relationship to functional abilities. *J Neurol Neurosurg Psychiatry.* 1994;57(2):202-7.
7. Hu G-C, Chen Y.-M. Post-stroke Dementia: Epidemiology, Mechanisms and Management. *International Journal of Gerontology.* 2017;11(4):210-4.
8. Zhao C, Deng W, and Gage FH. Mechanisms and functional implications of adult neurogenesis. *Cell.* 2008;132(4):645-60.
9. Akers KG, Martinez-Canabal A, Restivo L, Yiu AP, De Cristofaro A, Hsiang HL, et al. Hippocampal neurogenesis regulates forgetting during adulthood and infancy. *Science.* 2014;344(6184):598-602.
10. Mu Y, and Gage FH. Adult hippocampal neurogenesis and its role in Alzheimer's disease. *Mol Neurodegener.* 2011;6:85.

11. Cho KO, Lybrand ZR, Ito N, Brulet R, Tafacory F, Zhang L, et al. Aberrant hippocampal neurogenesis contributes to epilepsy and associated cognitive decline. *Nat Commun.* 2015;6:6606.
12. Schreglmann SR, Regensburger M, Rockenstein E, Masliah E, Xiang W, Winkler J, et al. The temporal expression pattern of alpha-synuclein modulates olfactory neurogenesis in transgenic mice. *PLoS One.* 2015;10(5):e0126261.
13. Aimone JB, Li Y, Lee SW, Clemenson GD, Deng W, and Gage FH. Regulation and function of adult neurogenesis: from genes to cognition. *Physiol Rev.* 2014;94(4):991-1026.
14. Lichtenwalner RJ, and Parent JM. Adult neurogenesis and the ischemic forebrain. *J Cereb Blood Flow Metab.* 2006;26(1):1-20.
15. Kernie SG, and Parent JM. Forebrain neurogenesis after focal Ischemic and traumatic brain injury. *Neurobiol Dis.* 2010;37(2):267-74.
16. Raber J, Fan Y, Matsumori Y, Liu Z, Weinstein PR, Fike JR, et al. Irradiation attenuates neurogenesis and exacerbates ischemia-induced deficits. *Ann Neurol.* 2004;55(3):381-9.
17. Sun C, Sun H, Wu S, Lee CC, Akamatsu Y, Wang RK, et al. Conditional ablation of neuroprogenitor cells in adult mice impedes recovery of poststroke cognitive function and reduces synaptic connectivity in the perforant pathway. *J Neurosci.* 2013;33(44):17314-25.
18. Niv F, Keiner S, Krishna, Witte OW, Lie DC, and Redecker C. Aberrant neurogenesis after stroke: a retroviral cell labeling study. *Stroke.* 2012;43(9):2468-75.
19. Woitke F, Ceanga M, Rudolph M, Niv F, Witte OW, Redecker C, et al. Adult hippocampal neurogenesis poststroke: More new granule cells but aberrant morphology and impaired spatial memory. *PLoS One.* 2017;12(9):e0183463.
20. Epp JR, Silva Mera R, Kohler S, Josselyn SA, and Frankland PW. Neurogenesis-mediated forgetting minimizes proactive interference. *Nat Commun.* 2016;7:10838.

21. Al-Qazzaz NK, Ali SH, Ahmad SA, Islam S, and Mohamad K. Cognitive impairment and memory dysfunction after a stroke diagnosis: a post-stroke memory assessment. *Neuropsychiatr Dis Treat.* 2014;10:1677-91.
22. Anagnostaras SG, Gale GD, and Fanselow MS. Hippocampus and contextual fear conditioning: recent controversies and advances. *Hippocampus.* 2001;11(1):8-17.
23. Altman J, and Das GD. Autoradiographic and histological evidence of postnatal hippocampal neurogenesis in rats. *J Comp Neurol.* 1965;124(3):319-35.
24. Kempermann G, Kuhn HG, and Gage FH. More hippocampal neurons in adult mice living in an enriched environment. *Nature.* 1997;386(6624):493-5.
25. van Praag H, Kempermann G, and Gage FH. Running increases cell proliferation and neurogenesis in the adult mouse dentate gyrus. *Nat Neurosci.* 1999;2(3):266-70.
26. Arvidsson A, Kokaia Z, and Lindvall O. N-methyl-D-aspartate receptor-mediated increase of neurogenesis in adult rat dentate gyrus following stroke. *Eur J Neurosci.* 2001;14(1):10-8.
27. Kluska MM, Witte OW, Bolz J, and Redecker C. Neurogenesis in the adult dentate gyrus after cortical infarcts: effects of infarct location, N-methyl-D-aspartate receptor blockade and anti-inflammatory treatment. *Neuroscience.* 2005;135(3):723-35.
28. Maekawa M, Namba T, Suzuki E, Yuasa S, Kohsaka S, and Uchino S. NMDA receptor antagonist memantine promotes cell proliferation and production of mature granule neurons in the adult hippocampus. *Neurosci Res.* 2009;63(4):259-66.
29. Girardeau G, Benchenane K, Wiener SI, Buzsaki G, and Zugaro MB. Selective suppression of hippocampal ripples impairs spatial memory. *Nat Neurosci.* 2009;12(10):1222-3.
30. Dupret D, O'Neill J, Pleydell-Bouverie B, and Csicsvari J. The reorganization and reactivation of hippocampal maps predict spatial memory performance. *Nat Neurosci.* 2010;13(8):995-1002.

31. Shapiro LA, Upadhyaya P, and Ribak CE. Spatiotemporal profile of dendritic outgrowth from newly born granule cells in the adult rat dentate gyrus. *Brain Res.* 2007;1149:30-7.
32. Llorens-Martin M, Jurado-Arjona J, Avila J, and Hernandez F. Novel connection between newborn granule neurons and the hippocampal CA2 field. *Exp Neurol.* 2015;263:285-92.
33. Imayoshi I, Ohtsuka T, Metzger D, Chambon P, and Kageyama R. Temporal regulation of Cre recombinase activity in neural stem cells. *Genesis.* 2006;44(5):233-8.
34. Kobayakawa K, Kobayakawa R, Matsumoto H, Oka Y, Imai T, Ikawa M, et al. Innate versus learned odour processing in the mouse olfactory bulb. *Nature.* 2007;450(7169):503-8.
35. Kobayashi Y, Sano Y, Vannoni E, Goto H, Suzuki H, Oba A, et al. Genetic dissection of medial habenula-interpeduncular nucleus pathway function in mice. *Front Behav Neurosci.* 2013;7:17.
36. Gorelick PB, Scuteri A, Black SE, Decarli C, Greenberg SM, Iadecola C, et al. Vascular contributions to cognitive impairment and dementia: a statement for healthcare professionals from the american heart association/american stroke association. *Stroke.* 2011;42(9):2672-713.
37. Iadecola C. The pathobiology of vascular dementia. *Neuron.* 2013;80(4):844-66.
38. Ming GL, and Song H. Adult neurogenesis in the mammalian central nervous system. *Annu Rev Neurosci.* 2005;28:223-50.
39. Spalding KL, Bergmann O, Alkass K, Bernard S, Salehpour M, Huttner HB, et al. Dynamics of hippocampal neurogenesis in adult humans. *Cell.* 2013;153(6):1219-27.
40. Zhao C, Teng EM, Summers RG, Jr., Ming GL, and Gage FH. Distinct morphological stages of dentate granule neuron maturation in the adult mouse hippocampus. *J Neurosci.* 2006;26(1):3-11.

41. Toni N, Teng EM, Bushong EA, Aimone JB, Zhao C, Consiglio A, et al. Synapse formation on neurons born in the adult hippocampus. *Nat Neurosci.* 2007;10(6):727-34.
42. Toni N, Laplagne DA, Zhao C, Lombardi G, Ribak CE, Gage FH, et al. Neurons born in the adult dentate gyrus form functional synapses with target cells. *Nat Neurosci.* 2008;11(8):901-7.
43. Gu Y, Arruda-Carvalho M, Wang J, Janoschka SR, Josselyn SA, Frankland PW, et al. Optical controlling reveals time-dependent roles for adult-born dentate granule cells. *Nat Neurosci.* 2012;15(12):1700-6.
44. Winner B, and Winkler J. Adult neurogenesis in neurodegenerative diseases. *Cold Spring Harb Perspect Biol.* 2015;7(4):a021287.
45. Frankland PW, Kohler S, and Josselyn SA. Hippocampal neurogenesis and forgetting. *Trends Neurosci.* 2013;36(9):497-503.
46. Restivo L, Niibori Y, Mercaldo V, Josselyn SA, and Frankland PW. Development of Adult-Generated Cell Connectivity with Excitatory and Inhibitory Cell Populations in the Hippocampus. *J Neurosci.* 2015;35(29):10600-12.
47. Lisman JE. Role of the dual entorhinal inputs to hippocampus: a hypothesis based on cue/action (non-self/self) couplets. *Prog Brain Res.* 2007;163:615-25.
48. Acsady L, Kamondi A, Sik A, Freund T, and Buzsaki G. GABAergic cells are the major postsynaptic targets of mossy fibers in the rat hippocampus. *J Neurosci.* 1998;18(9):3386-403.
49. Schmidt-Hieber C, Jonas P, and Bischofberger J. Enhanced synaptic plasticity in newly generated granule cells of the adult hippocampus. *Nature.* 2004;429(6988):184-7.
50. Ge S, Yang CH, Hsu KS, Ming GL, and Song H. A critical period for enhanced synaptic plasticity in newly generated neurons of the adult brain. *Neuron.* 2007;54(4):559-66.

51. Nakatomi H, Kuriu T, Okabe S, Yamamoto S, Hatano O, Kawahara N, et al. Regeneration of hippocampal pyramidal neurons after ischemic brain injury by recruitment of endogenous neural progenitors. *Cell.* 2002;110(4):429-41.
52. Bendel O, Bueters T, von Euler M, Ove Ogren S, Sandin J, and von Euler G. Reappearance of hippocampal CA1 neurons after ischemia is associated with recovery of learning and memory. *J Cereb Blood Flow Metab.* 2005;25(12):1586-95.
53. Luo CX, Jiang J, Zhou QG, Zhu XJ, Wang W, Zhang ZJ, et al. Voluntary exercise-induced neurogenesis in the postischemic dentate gyrus is associated with spatial memory recovery from stroke. *J Neurosci Res.* 2007;85(8):1637-46.
54. Li WL, Cai HH, Wang B, Chen L, Zhou QG, Luo CX, et al. Chronic fluoxetine treatment improves ischemia-induced spatial cognitive deficits through increasing hippocampal neurogenesis after stroke. *J Neurosci Res.* 2009;87(1):112-22.
55. van Praag H. Neurogenesis and exercise: past and future directions. *Neuromolecular Med.* 2008;10(2):128-40.
56. Tsai YW, Yang YR, Wang PS, and Wang RY. Intermittent hypoxia after transient focal ischemia induces hippocampal neurogenesis and c-Fos expression and reverses spatial memory deficits in rats. *PLoS One.* 2011;6(8):e24001.
57. Malberg JE, Eisch AJ, Nestler EJ, and Duman RS. Chronic antidepressant treatment increases neurogenesis in adult rat hippocampus. *J Neurosci.* 2000;20(24):9104-10.
58. Ishikawa R, Fukushima H, Frankland PW, and Kida S. Hippocampal neurogenesis enhancers promote forgetting of remote fear memory after hippocampal reactivation by retrieval. *Elife.* 2016;5.
59. Shi J, Miles DK, Orr BA, Massa SM, and Kernie SG. Injury-induced neurogenesis in Bax-deficient mice: evidence for regulation by voltage-gated potassium channels. *Eur J Neurosci.* 2007;25(12):3499-512.
60. Mattson MP. Glutamate and neurotrophic factors in neuronal plasticity and disease. *Ann N Y Acad Sci.* 2008;1144:97-112.

61. Myer DJ, Gurkoff GG, Lee SM, Hovda DA, and Sofroniew MV. Essential protective roles of reactive astrocytes in traumatic brain injury. *Brain.* 2006;129(Pt 10):2761-72.

62. Bessis A, Bechade C, Bernard D, and Roumier A. Microglial control of neuronal death and synaptic properties. *Glia.* 2007;55(3):233-8.

63. Mignone JL, Kukekov V, Chiang AS, Steindler D, and Enikolopov G. Neural stem and progenitor cells in nestin-GFP transgenic mice. *J Comp Neurol.* 2004;469(3):311-24.

64. Ballesteros I, Cuartero MI, Moraga A, de la Parra J, Lizasoain I, and Moro MA. Stereological and flow cytometry characterization of leukocyte subpopulations in models of transient or permanent cerebral ischemia. *J Vis Exp.* 2014(94).

65. Cuartero MI, Ballesteros I, de la Parra J, Harkin AL, Abautret-Daly A, Sherwin E, et al. L-kynurenine/aryl hydrocarbon receptor pathway mediates brain damage after experimental stroke. *Circulation.* 2014;130(23):2040-51.

66. Garthe A, Behr J, and Kempermann G. Adult-generated hippocampal neurons allow the flexible use of spatially precise learning strategies. *PLoS One.* 2009;4(5):e5464.

67. Kitamura T, Saitoh Y, Takashima N, Murayama A, Niibori Y, Ageta H, et al. Adult neurogenesis modulates the hippocampus-dependent period of associative fear memory. *Cell.* 2009;139(4):814-27.

68. Ferreira T, Ou Y, Li S, Giniger E, and van Meyel DJ. Dendrite architecture organized by transcriptional control of the F-actin nucleator Spire. *Development.* 2014;141(3):650-60.

## FIGURES AND FIGURE LEGENDS

**Figure 1. Cortical stroke impairs long-term memory in mice. (A)** Experimental design for panels B-C. Sham and MCAO mice were subjected to contextual fear conditioning (CFC; 0.6mA x 3) and tested 28 and 60 days after training. **(B-C)** Remote memory retention after cerebral ischemia calculated as the % of freezing response 28d (B; $p<0.05$ vs. sham; sham, n=37; MCAO, n=63) and 60 days (C: *$p<0.05$ vs. sham group; sham, n=8; MCAO, n=8) after foot-shocks. **(D)** Experimental design for panels E and F. **(E)** Percentage of freezing in control and MCAO groups after a weak (0.4mA x 2; left columns; light orange panel; *$p<0.05$ vs. sham group; sham, n=7; MCAO, n=7) or a strong fear conditioning paradigm (0.8mA x 5; right columns; dark orange panel; $p>0.05$ vs. sham group; sham, n=5; MCAO, n=5). Retention for both types of conditioning was performed 28 days after training and 60 days after conditioning for the strong one. **(F)** Memory persistence at 2 months of strong fear conditioning paradigm. Data is represented as % of freezing at 2 months versus that observed at 1 month (*$p<0.05$ vs. sham group; sham, n=5; MCAO, n=5). **(G-H)** Freezing response after conditioning (0.6mA x 3) performed 48 hours before surgery (G: *$p<0.05$ vs. sham; sham, n=9; MCAO, n=7) or 30d after MCAO (H: *$p<0.05$ vs. sham; sham, n=15; MCAO, n=15), respectively. Data are mean ± SEM. Data were compared using nonparametric 2-tailed Mann-Whitney tests.

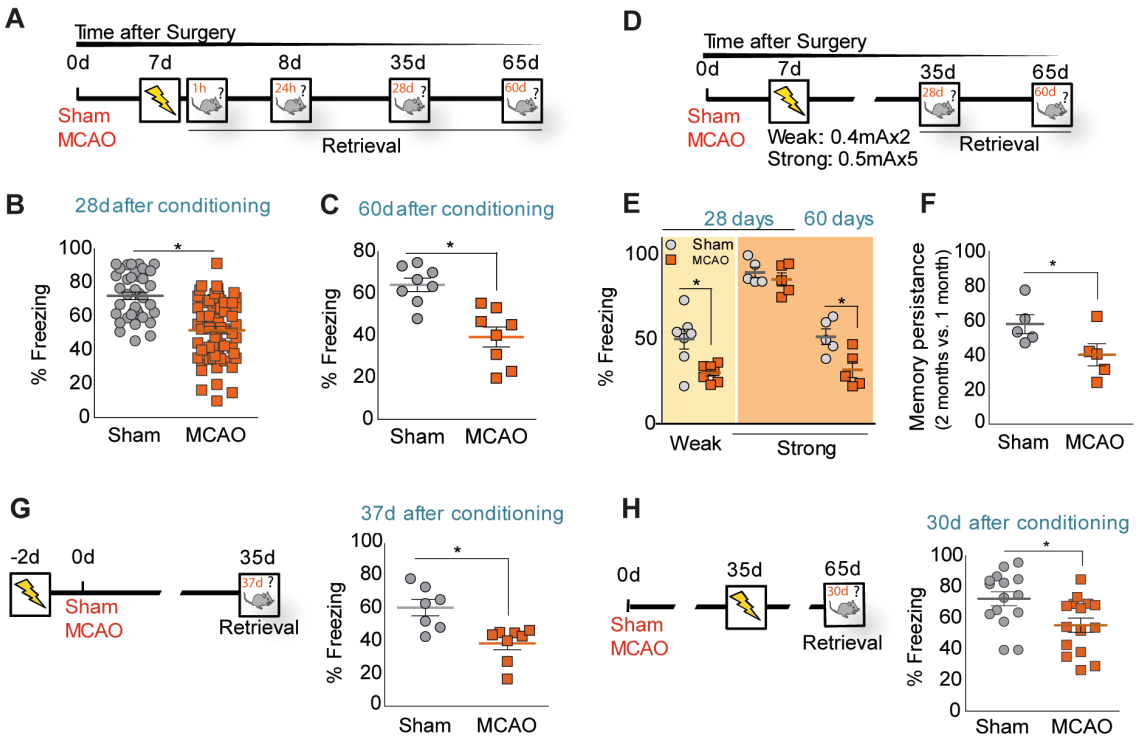

**Figure 2. Long-term memory deficits after MCAO are hippocampus-dependent. (A)** Design for hippocampus inactivation with tetrodotoxin (TTX) before retrieval of fear memory. Sham and MCAO mice were subjected to CFC (0.6mA x 3) 7 days after surgery and tested 28 days after training (*p<0.05 vs. sham; sham, n=9; MCAO, n=13). One day later, sham and MCAO mice, allocated in two different groups, were bilaterally infused in the dorsal hippocampus with either vehicle or TTX. Three hours later, fear memory was evaluated as % of freezing (sham veh, n=4; MCAO veh, n=5; sham TTX, n=5; MCAO TTX, n=8; *p<0.05 vs. sham veh; #p<0.05 vs. MCAO veh; ns, no significant). **(B)** Representative images of c-Fos staining (green) in the hippocampus of untrained, sham and ischemic mice 90 minutes after a 10-min retrieval session, 28d after conditioning. Scale bar: 200µm. **(C-F)** Barnes maze testing. (C) Experimental design. (D) Representative traces of the paths travelled during retrieval by mice in the Barnes maze obtained by Ethowatcher software. Time spent by sham and MCAO mice around each quadrant (E) or around the target hole (F) in the Barnes maze platform 30d after training. In (E), two-way ANOVA showed a significant interaction between quadrants and surgery ($F(3,116)=3.50$; $p=0.0178$) (Bonferroni post-hoc: *p<0.05 vs. sham TQ; sham, n=12; MCAO; n=19). TQ, RQ, ATQ and LQ (target, right, anti-target and left quadrant, respectively). In (F), *p<0.05 vs. sham group. Data are mean ± SEM. Data were compared by using nonparametric 2-tailed Mann-Whitney tests (A and F) or a nonparametric 2-way ANOVA followed by Bonferroni post hoc testing (E).

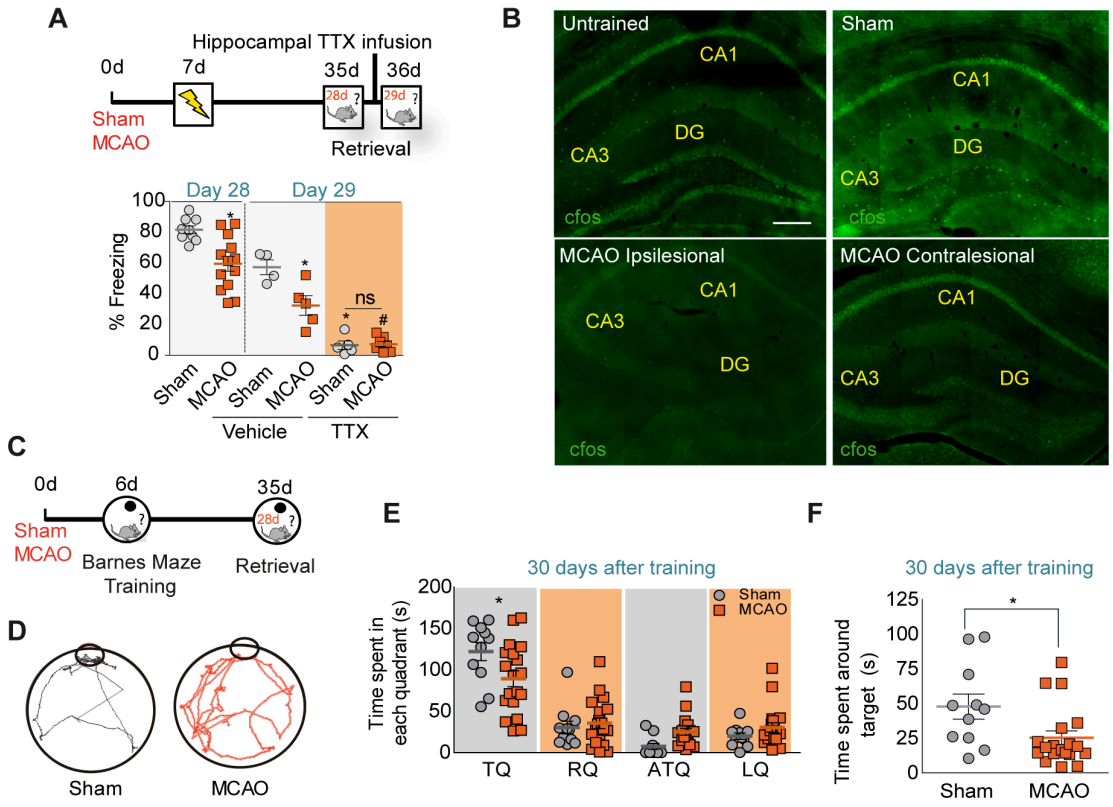

**Figure 3. Hippocampal neurogenesis positively correlates with memory impairment. (A-B)** Cavalieri estimation of granular cell layer (GCL) volume in Nissl-stained sections from sham and MCAO mice 35 days after surgery (*p<0.05 vs. sham; sham, n=10; MCAO, n=40). Representative images are shown in (B). Scale bar: 100µm. **(C)** Negative relationship between GCL volume and % of freezing response in the ischemic group. Linear regression analysis is displayed in the graph (MCAO, n=44; Spearman r=-0.4972, p=0.0016). **(D)** Experimental design for Ki67, DCX and BrdU quantification after different time points of stroke onset. **(E-H)** Quantification of proliferative Ki67$^+$ cells (F) and DCX$^+$ immature neurons (H) in sham and MCAO mice (ipsi- and contralesional DG). In (F), a significant interaction between time after ischemic onset and ischemia was found for Ki67$^+$ ($F_{(10,59)}$= 3.5; p=0.0010; Bonferroni post-hoc: *p<0.05 vs. sham; sham, n=4-5; MCAO ipsilesional, n=4-5; MCAO contralesional, n=3-5). In (H), two-way ANOVA showed significant differences for ischemia ($F_{(2,57)}$= 27.90; p<0.0001) and for time after ischemic onset ($F_{(5,57)}$= 5.57; p<0.0001) (Bonferroni post-hoc: *p<0.05 vs. sham; sham, n=3-5; MCAO ipsilesional, n=3-5; MCAO contralesional, n=3-5). (E) and (G) show representative images of Ki67$^+$ (red) and DCX$^+$ cells (green), respectively, 14d and 35 days after surgery. Scale bar: 30µm. **(I-J)** Spearman correlation between ipsilesional DCX$^+$ cells and % of freezing at 35d after surgery in ischemic mice (I, MCAO, n=66; Spearman r=-0.651, p<0.0001) or between DCX$^+$ cells and GCL volume in ischemic mice (MCAO, n=40; Spearman r=0.4177, p=0.0059). Data are mean ± SEM. Data were compared by using nonparametric 2-tailed Mann-Whitney tests (A), a nonparametric 2-way ANOVA followed by Bonferroni post hoc testing (E and G), and correlation analysis was assessed by Spearman (C, I and J).

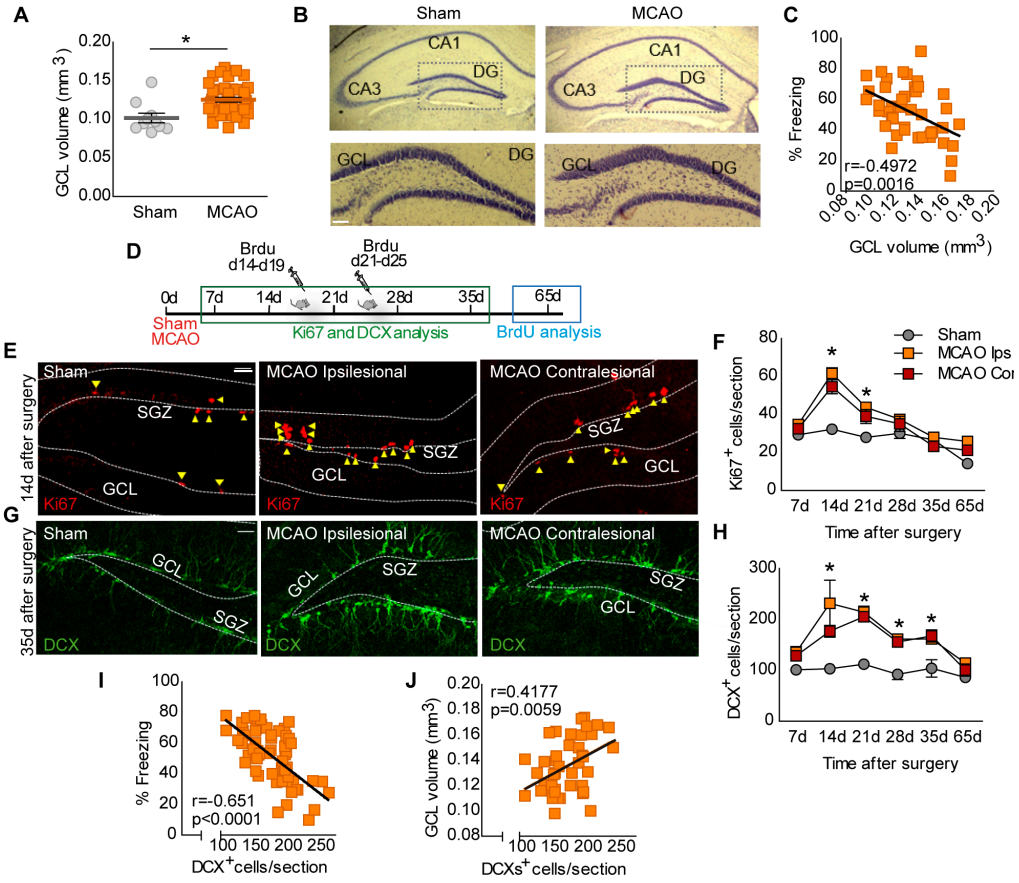

**Figure 4. Increasing post-stroke neurogenesis enhance cognitive impairment**. **(A-D)** Quantification of Ki67$^+$ (A) and DCX$^+$ cells (C) 35d after surgery in sedentary and runner MCAO mice. Representative images of Ki67$^+$ (B, red) and DCX$^+$ cells (D, green) in sedentary and runner MCAO mice. Scale bar: 30µm. Two-way ANOVA analysis showed significant effect of running in the number of Ki67$^+$ (A) ($F_{(1,30)}$= 50.09; p<0.0001) and DCX$^+$ cells (C) ($F_{(1,29)}$= 14.05; p=0.0008) in ipsi- and contralesional sides (Bonferroni post-hoc: *p<0.05 vs. MCAO sedentary; MCAO sedentary, n=8; MCAO runner, n=9). **(E)** MCAO mice remained sedentary or ran after CFC and were tested 28d after (*p<0.05 vs. MCAO sedentary; MCAO sedentary, n=13; MCAO runner, n=8). **(F-I)** Barnes maze testing. (F) Experimental design. (G) Representative traces. Time spent by sedentary and runner MCAO mice around each quadrant (H) or the target hole (I) during testing. In (H), two-way ANOVA demonstrated a significant interaction between different quadrants and running (F(3,96)= 3.25; p=0.0251); *p<0.05 vs. MCAO sedentary TQ; Bonferroni post-test). In (I), *p<0.05 vs. MCAO sedentary; MCAO sedentary, n=15; MCAO runner, n=11). **(J-L)** MCAO mice treated with memantine (MEM) showed a reduced freezing response 28d after training (L) (*p<0.05 vs. MCAO vehicle; MCAO vehicle, n=7; MCAO MEM, n=11) and increased the number of DCX$^+$ cells in ipsi- and contralesional hippocampus (J-K). (J) Two-way ANOVA demonstrated significant effect of MEM in DCX$^+$ cells ($F_{(1,33)}$= 28.85; p<0.0001) in ipsi- and contralesional hippocampus (Bonferroni post-hoc: *p<0.05 vs. MCAO vehicle; MCAO vehicle, n=7; MCAO MEM, n=10). Representative images of DCX$^+$ cells (K). Scale bar: 30µm. Data are mean ± SEM. Data were compared by using nonparametric 2-tailed Mann-Whitney tests (E, I and L), a nonparametric 2-way ANOVA followed by Bonferroni post hoc testing (A, C, H and J).

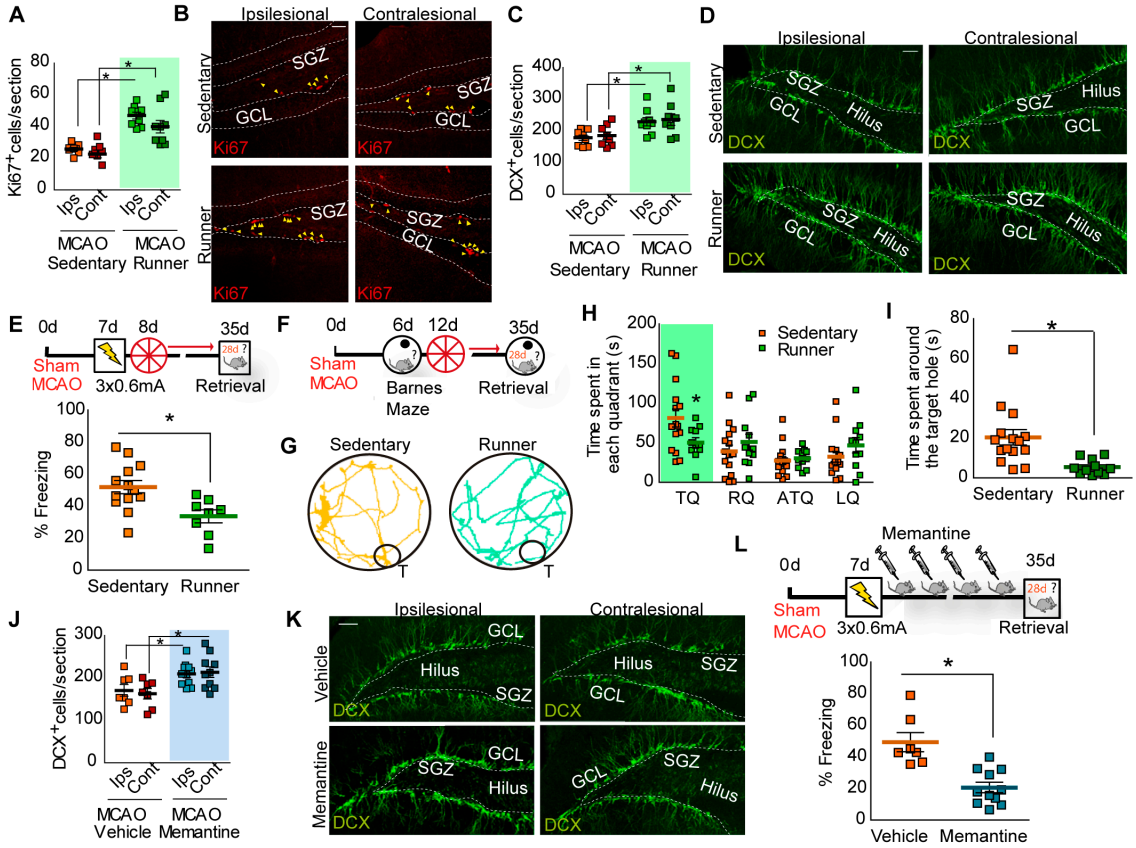

**Figure 5. Altered features of newborn neurons induced by stroke. (A)** Experimental design for labelling new generated neurons after stroke by a GFP retrovirus. **(B)** Representative images of GFP newborn neurons of each group. Yellow arrow: 112µm. **(C)** Sholl analysis of GFP-retrovirally infected newborn neurons in the DG of sham and MCAO, 28 days after infection. Two-way ANOVA of Sholl analysis demonstrates a significant interaction between distance and experimental group in the number of intersections ($F_{(48,3022)}$= 5.18; p<0.0001; Bonferroni post-hoc: *#p<0.05 vs. sham and MCAO ipsilesional, respectively; sham, n=52 neurons/4 mice; MCAO ipsilesional, n=41neurons/4mice; MCAO contralesional, n=32neurons/3mice). **(D)** Mean averaged intersections of GFP neurons estimated in different intervals from soma. From left to right: 0-50µm; 60-140µm and 150-250µm (*#p<0.05 vs. sham and MCAO ipsilesional, respectively; sham, n=52 neurons/4 mice; MCAO ipsilesional, n=41neurons/4mice; MCAO contralesional, n=32neurons/3mice). **(E-F)** Quantification of total dendritic length (E; *#p<0.05 vs. sham and MCAO ipsilesional, respectively; sham, n=18 neurons/4 mice; MCAO ipsilesional, n=45neurons/4 mice; MCAO contralesional, n=29neurons/3mice) and apical dendritic length (J: *#p<0.05 vs. sham and MCAO ipsilesional, respectively; sham, n=61 neurons/4 mice; MCAO ipsilesional, n=60neurons/4mice; MCAO contralesional, n=40neurons/3mice) in sham and both ipsi- and contralesional sides of MCAO group. **(G)** Pie charts display the percentage of $GFP^+$ neurons in each experimental group showing apical dendrite lengths of <10µm, 10-40µm and >40µm (sham, n=61 neurons/4mice; MCAO ipsilesional n=60neurons/4mice; MCAO contralesional, n=40neurons/3mice). Data are mean ± SEM. Data were compared by using nonparametric 2-tailed Mann-Whitney tests (D, E and F), a nonparametric 2-way ANOVA followed by Bonferroni post hoc testing (C).

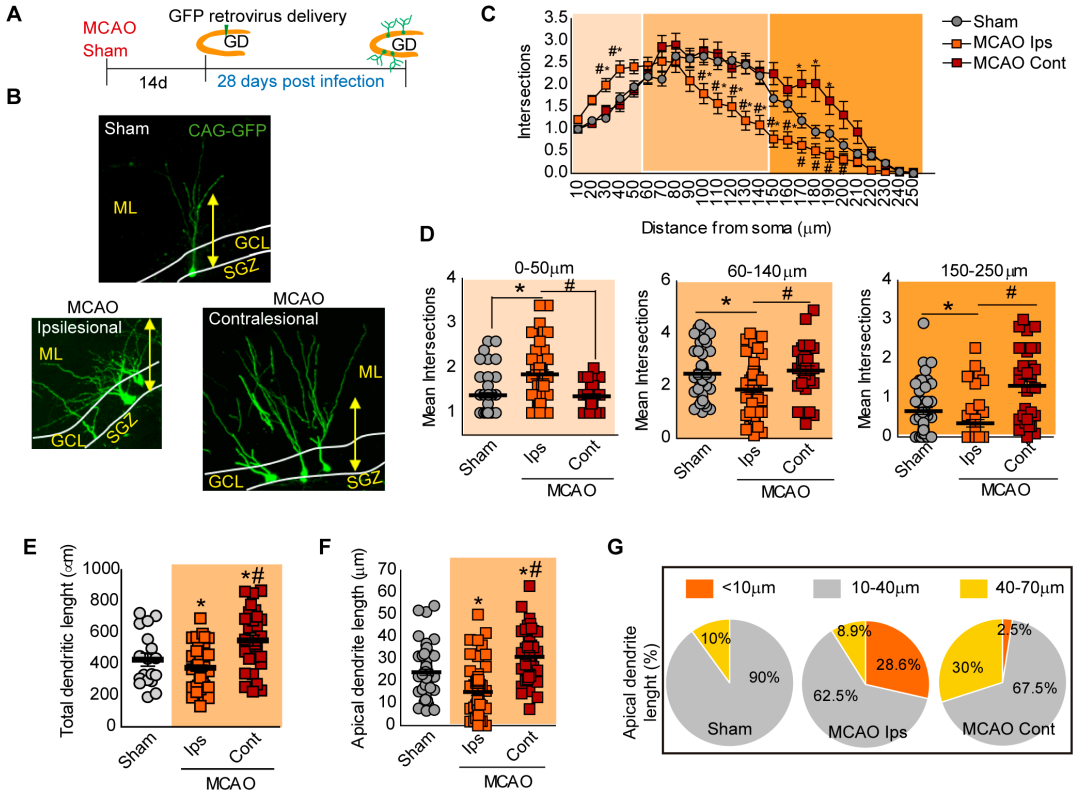

**Figure 6. Temozolomide treatment after stroke mitigates hippocampus-dependent memory deficits. (A-B)** Number of $DCX^+$ cells in MCAO mice treated with vehicle or either with temozolomide (TMZ). Representative images of $DCX^+$ cells (B; green) in MCAO mice treated with vehicle or TMZ. Scale bar: 30µm. In A, two-way ANOVA analysis showed a significant effect of TMZ in the number of $DCX^+$ cells ($F_{(1,32)}$= 81.85; p<0.0001) in both ipsi- and contralesional sides (Bonferroni post-hoc: *p<0.05 vs. MCAO vehicle; MCAO vehicle, n=8; MCAO TMZ, n=9) at 35 days. **(C)** Experimental design for post-stroke neurogenesis inhibition by TMZ. Seven days after ischemia, mice were subjected to contextual fear conditioning (0.6mA x 3) and 24h later, they were treated i.p. with TMZ (25mg/Kg) for 4 weeks (3 days per week) and tested in the CFC at the end of the treatment. **(D)** Percentage of freezing response in vehicle- or TMZ-treated ischemic mice 35 days after contextual fear conditioning (*p<0.05 vs. MCAO vehicle; MCAO vehicle, n=13; MCAO TMZ, n=9). Data are mean ± SEM. Data were compared by using nonparametric 2-tailed Mann-Whitney tests (D), a nonparametric 2-way ANOVA followed by Bonferroni post hoc testing (A).

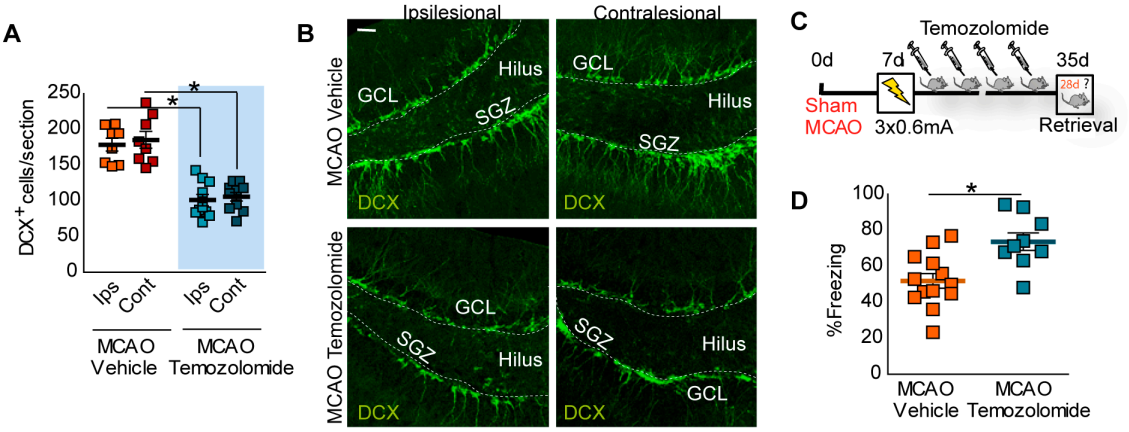

**Figure 7. Conditional deletion of newborn neurons after stroke decreases cognitive deficits. (A)** Genetic strategy used for conditional deletion of newborn neurons after stroke. **(B)** Number of $DCX^+$ cells in MCAO Nestin-$Cre^{ERT2}$/NSE-DTA mice treated with vehicle or tamoxifen. Two-way ANOVA showed a significant effect of tamoxifen in the number of $DCX^+$ cells ($F_{(1,48)}$= 136.59; p<0.0001) in both ipsi- and contralesional sides (Bonferroni post-hoc: *p<0.05 vs. Nes-$Cre^{ERT2}$/NSE-DTA vehicle; vehicle, n=14; tamoxifen, n=12). **(C)** Representative images of $DCX^+$ cells (green) in ischemic Nestin-$Cre^{ERT2}$/NSE-DTA mice after vehicle or tamoxifen 35 days after surgery. Scale bar: 30µm. **(D)** Percentage of freezing in vehicle- or tamoxifen-Nestin-$Cre^{ERT2}$/NSE-DTA treated mice 35 days after contextual fear conditioning (*p<0.05 vs. Nestin-$Cre^{ERT2}$/NSE-DTA vehicle; vehicle, n=12 and tamoxifen, n=13). Top: Experimental design. Seven days after ischemia, Nestin-$Cre^{ERT2}$/NSE-DTA mice were subjected to contextual fear conditioning (0.6mA x 3) and 24h later they were treated i.p with vehicle or tamoxifen (150mg/Kg) during 4 consecutive days and tested in the CFC 35 days after surgery. **(E-H)** Experimental design for assessing spatial memory retention in the Barnes maze (E). Five days after ischemia, Nestin-$Cre^{ERT2}$/NSE-DTA mice were trained during 7 days (3 session/day) into the Barnes maze. After training, mice were treated with vehicle or tamoxifen and tested 28 days later. (F) Representative traces during the retention test. (G) Time spent in each quadrant of the Barnes maze platform. Two-way ANOVA demonstrated a significant interaction between quadrants and tamoxifen treatment in ischemic Nestin-$Cre^{ERT2}$/NSE-DTA ($F_{(3,68)}$= 4.41; p=0.0068; Bonferroni post-test: *p<0.05 vs. Nestin-$Cre^{ERT2}$/NSE-DTA vehicle TQ). (H) Time spent around target hole during testing (*p<0.05 vs. MCAO Nestin-$Cre^{ERT2}$/NSE-DTA vehicle; vehicle, n=7; tamoxifen, n=12). Data are mean ± SEM. Data were compared by using nonparametric 2-tailed Mann-Whitney tests (D and H) and a nonparametric 2-way ANOVA followed by Bonferroni post hoc testing (B and G).